



# Time-resolved fluorescence and anisotropy studies of red pigments present in acrylic formulations

Andrea Cadena-Caicedo, Mario González-Gutiérrez, Óscar Guzmán-Méndez, Mariana M. Reza, Jesús Durán-Hernández, Jorge Peon\*

Instituto de Química, Universidad Nacional Autónoma de México, Circuito Exterior, Ciudad Universitaria, Ciudad de México, 04510, Mexico

## ARTICLE INFO

### Keywords:

Pigments  
Fluorescent  
Perylene  
Quinacridone  
Time-correlated single photon counting  
Time-Resolved Emission Anisotropy  
Minimal sample

## ABSTRACT

Red organic pigments are frequently found in modern paintings and murals based on acrylic formulations. The detection of these molecules is valuable to guide investigations about cultural heritage and for restoration efforts. These studies usually employ microscopic amounts of materials that are obtained through swabbing or micro-sampling. In this contribution we describe the time-resolved emission properties of a set of red pigments with the objective of characterizing their excited state properties and developing strategies to identify their presence through fluorescence lifetime measurements, even in concentrations of the order of  $10^{-9}$  M. As we show, using different solvent systems, the emission decay measurements can be setup to be a robust identification technique that avoids problems with evaporation or partial solubility. We also show that the sensitivity of these determinations is improved using a confocal type of setup with a high numerical aperture lens to ensure a high photon capture. This setup also allows for the samples to be prepared in microliter level volumes which implies a relatively high concentration of the pigments. In addition, we show that the lifetime measurements can be complemented with determinations of the emission anisotropy decays with the same experimental setup, which provides an additional property specific to each pigment, permitting an accurate differentiation between fluorophores.

## 1. Introduction

The development of acrylic paints as an artistic medium emerged in Mexico in the 1920s. With these materials, artists like David Alfaro Siqueiros, Diego Rivera and José Clemente Orozco found a solution to the problem of an environment-resistant media to shape public large-scale artworks [1]. Acrylics are still in use nowadays by modern artists due to their coloring effects, fast drying and permanence qualities [2]. A frequent motif of artwork based on acrylic paints is the use of bright red organic pigments which frequently appear as a single coloring agent in the formulation which can be dispersed through large areas of a mural [3,4]. The study and identification of these pigments, which are defined as non-soluble dyes in the medium and provide opacity and color properties [3], can be important for conservation and restoration purposes [5–11]. Usually, the historical background of a particular art piece or mural will yield a small set of options to discern the specific pigment [12]. Recent developments in separative analytical chemistry have made it possible to identify organic pigments in artworks [13–15].

However, in most cases, the analysis of historical samples by methods based in chromatographic analysis is affected by the requirement of relatively large samples (0.5–1 mg) since the content of the organic colorants only corresponds to a few percent of the sample mass [16].

In recent years, techniques based on the use of visible light have been advanced to determine the presence of specific components in artworks [12,14,15,17–28]. Optical spectroscopic techniques have specific advantages for some of these applications, which may include portability and direct use on the art piece, or the possibility of combining different methods like reflectance, absorbance and emission spectroscopies [12, 20,29–32]. Despite the availability of different optical methods, the unparallel sensitivity of fluorescence spectroscopy has not been fully taken advantage of, due to the fact that the emission bands of conjugated systems tend to be broad and featureless [29,33,34]. In this regard, time-resolved fluorescence measurements can provide significant additional information for microscopic samples dissolved in small solvent volumes, which may be obtained from minimal-contact swabbing [35–37], microscopic flakes, or as fractions from micro-scale separation

\* Corresponding author. Universidad Nacional Autónoma de México, Instituto de Química, Ciudad Universitaria, 04510, México, DF, Mexico.  
E-mail address: [jpeon@unam.mx](mailto:jpeon@unam.mx) (J. Peon).

methods [38].

Time-resolved emission measurements through Time-Correlated Single Photon Counting (TCSPC) is based on the correlation of individually detected photons to build a histogram of their emission times after a short excitation light pulse. Due to the high sensitivity of modern avalanche photodiode detectors (APDs), and the high fraction of photons that can be brought to the detector with high numerical aperture (NA) objectives (see below), TCSPC is among the spectroscopic techniques with the highest sensitivity for emissive molecules [29,39,40]. Of importance for the present study, the use of high numerical aperture objectives -where the excitation and light collection is made with the same lens system-also allows for a drastic reduction of the volume of the dissolved sample, down the order of a microliter. With this volume level, a high concentration of the fluorophores can be achieved even when the original sample might be of the order of a few picomoles [39,41], including cases where the sample is obtained through the use of a small sampling swab (micro-swab) dabbed on the surface of the material by an expert art restorer (also, see video linked through the Supporting Info.) [35–37,42,43]. In addition, if the sample is obtained as a chromatographic fraction, the solvent can be appropriately evaporated to increase the concentration of the emissive pigment [38,44].

In this contribution we highlight several issues related to the use of TCSPC to identify the presence of emissive organic red pigments in acrylic formulations. Nowadays, TCSPC is a common technique available in commercial fluorimeters and has been used previously for heritage studies [29]. We seek to comment on the sensitivity of this technique, and to explore different variables and strategies for the use of setups which are similar to a confocal setup but without a detection pinhole to increase sensitivity. This arrangement makes it possible to time-resolve fluorescence signals with excellent signal-to-noise ratio in concentrations of the order of  $10^{-9}$  M from sample sizes less than  $100 \mu\text{m}^2$ , in volumes of the order of microliters. As we show, depending on the sample, the combination of different solvents for extraction and detection of the TCSPC sample can greatly improve the robustness of the method. In addition to TCSPC traces, we performed Time-Resolved Emission Anisotropy (TREA) measurements using the same setup to have an additional method to corroborate the presence of a given pigment and to differentiate between pigments that have similar decay times. The TREA decays are directly related to the rotational diffusion of the molecules in the solution. Thus, they are an additional signature of each molecule with a strong dependence on the solvent system. In fact, from proper adjustment of solvent mixtures, the anisotropy decays can

be made to fit in different time-regimes. This allows for a proper determination window which should be adequate for both the fluorescence lifetime of the molecule, and the time resolution of the instruments [39,41].

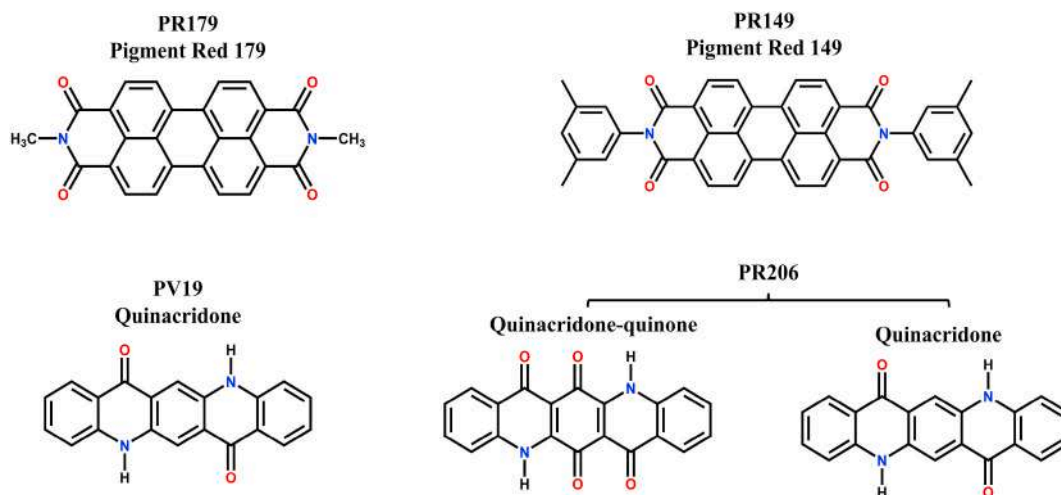
For this opening study, we have chosen a small set of red pigments, including quinacridones and diimides of the perylene tetracarboxylic acid contained in acrylic formulations frequently used in modern paintings. The molecular structures are included in Scheme 1. These compounds make up a test-set of pigments, which actually have been used in modern art works [8,18,45–48], and that were selected in order to foresee general strategies for the use of TCSPC in these purposes. Some examples of the specific use of these pigments by modern artists is documented in the Supporting Info.

The typical signals of these pigments were also determined from extractions of the respective commercial acrylic formulations: PR149, PR179, PR206 and PV19. Finally, these acrylics were sampled from dry surfaces using different substrates to explore the effects of the base surface on the measurements. As substrates we included plaster (P), fiber cement (FC), gray cement (GC) and white cement (WC).

## 2. Experimental

### 2.1. Materials and sample preparations

Pure pigments, commercial forms of the pigments and acrylic formulations were examined in this work. The pure pigments were either purchased directly or isolated from one of the commercial formulations. The commercial pigments were quinacridone chestnut brown-PR206 (Kremer Pigmente) and quinacridone red magenta-PV19 (Kremer Pigmente). The molecules purchased directly in pure form correspond to Pigment Red 149: N, N'-bis(3,5 dimethylphenyl)-3,4,9,10-perylenetetracarboxylic diimide, which was obtained from TCI AMERICA, and Pigment Red 179: N, N'-dimethyl-3,4,9,10-perylenedicarboximide which was obtained from Sigma Aldrich (also known as perylene maroon). The acrylic formulations of this study correspond to: Quinacridone red-PV19 (#7310, Golden acrylics), perylene maroon-PR179 (#507, Winsor & Newton acrylics), perylene red-PR149 (#464, Winsor & Newton acrylics), and quinacridone burnt orange-PR206 (#549, Winsor & Newton acrylics). For solvents we used dichloromethane (Sigma Aldrich, HPLC,  $\geq 99.8\%$ ), dimethyl sulfoxide (DMSO, Sigma Aldrich, for inorganic trace analysis,  $\geq 99.99995\%$ ), glycerin (Sigma Aldrich,  $\geq 99.5\%$ ) and toluene (Sigma Aldrich, 99.9%). For the cases of



**Scheme 1.** Structures of the pigments considered in this study. The labels indicate the formulation which contains the respective chromophore. In commercial products, it is frequent that the acrylic is directly labeled from the common or commercial name of the pigment. This is the case of PR179 (Pigment Red 179) and PR149 (Pigment Red 149). For the case of the PR206 formulation, it contains two chromophores: quinacridone-quinone (left) and quinacridone (right). For PV19 the only pigment present is quinacridone.

PV19 and PR206 the pure forms of the pigments were obtained by isolation from the commercial samples. The molecules were purified by column chromatography using dichloromethane and methanol for the elution procedure. The identity of the molecules purified by chromatography (quinacridones), as well as the pure perylenes (Pigment Red 149 and Pigment Red 179), were verified by mass spectrometry (see Supporting Info.), and steady-state spectroscopy [49–52]. Scheme 1 can be used for reference to these pigments and the respective acrylic formulations through this text. Pure and commercial pigment solutions at concentrations of  $2 \times 10^{-6}$  M, and the respective dilutions were prepared daily.

## 2.2. Acrylic samples from surfaces

200  $\mu$ m thick films were formed of each acrylic formulation. This was done following the ASTM D823-25 standard on a glass slide (“Blade” method) [53]. Each film was left to dry in the dark for one week. Sample extraction and handling were made with a needle. The samples ( $\sim 0.4 \times 0.4$  mm) were placed in microtubes with 2 mL of dichloromethane for PR149 and PR179, or DMSO for PV19 and PR206 depending on the solubility of the pigment. Then, the solutions were sonicated for 15 min and kept for 24 h in the dark. In all cases the supernatant was taken directly from the extract.

Cement surfaces (white and gray) with a size of  $80 \times 20$  mm were made from a water/cement mixture of 50 g of water and 125 g of cement. Rapid curing was carried out for these samples using a water bath at a temperature of  $25 \pm 3$  °C for 3 h. Curing took place in the laboratory in a humid place to avoid sudden changes in temperature that would impair the curing of the cement for a few days. For the plaster surfaces, one part of water was mixed with three parts of dry plaster. Then,  $80 \times 20$  mm plates were formed by applying the mixture onto cardboard surfaces, and dried for 48 h.

A fiber cement panel manufactured by the Cenpanel brand company model Procovers was used. Cenpanel is a registered trademark of Mexalit Industrias S.A. de C.V. and Grupo Eureka, a company that provided the painter David Alfaro Siqueiros with fiber cement panels for his production of mural works during the sixties and seventies.  $30 \times 15$  cm cuts were made by moistening the panel surface with distilled water to avoid the formation of fiber cement particles.

The acrylic formulations were applied to each surface obtaining coatings of approximately 200  $\mu$ m. Once dry, the extraction and manipulation of the sub-100  $\mu$ m lateral size samples were performed with the help of a Nikon SMZ 1500 zoom stereomicroscope with final magnifications of 7.5–112 X. The samples were dissolved in 500  $\mu$ L of the respective solvent for the time-resolved emission measurements. The size of the samples is shown in the Supporting Info. For the microscopic samples (below 100  $\mu$ m lateral size) that use dichloromethane as solvent, specific transfers into other solvents were made in order to eliminate changes in concentration during the measurements from evaporation effects. This is further described in the results section.

## 2.3. Steady-state spectroscopy

Absorption and fluorescence spectra were measured in a Cary-50 (Varian) spectrophotometer and a Cary Eclipse (Varian) fluorimeter respectively. All spectra were recorded at room temperature ( $20 \pm 1$  °C) in a 1 cm pathlength quartz cell. The fluorescence yields ( $\varphi_f$ ) of pigments in  $\text{CH}_2\text{Cl}_2$  or DMSO were obtained using the comparative method of Williams et al. [54], where 9,10-diphenylanthracene in ethanol has been used as a standard solution (fluorescence yield: 0.95) [55,56]. Finally, molar extinction coefficients ( $\epsilon$ ) at the maximum peak of pigments were determined considering the Lambert-Beer law.

## 2.4. Time-correlated single photon measurements

The measurements were made on a setup similar to a confocal

microscope built in conjunction with a TCSPC system [57–59]. A detailed diagram of the setup is included in Fig. S3 in the Supporting Info. In order to maximize the light brought into the detectors, these setups do not use a pinhole in the focal plane of the tube lens. A 485 nm ps pulsed-laser with a repetition frequency of 10 MHz (LDHD-C-485, PicoQuant) was used to excite the pigment solutions which were placed between a pair of cover slides in order to minimize the required sample volume which easily can be as small as a microliter. The pigment's fluorescence was collected with a 1.4 NA objective lens (Nikon Plan Apo VC 60 $\times$ /1.4 oil immersion DIC N2). The emission was filtered through a 510 nm long pass dichroic mirror (Chroma T510lpxrt-UF2). It should be noted that this dichroic is appropriate for the emission of all the pigments of this study as their emission wavelength falls within 25 nm of each other. Once the residual excitation photons were removed, the emission beam was directed and focused into an avalanche photodiode-APD (PD-050-CTE, Micro Photon Devices). The focusing was made with a 30 mm focal length lens in order to fit the entire focused spot on the active area of the detectors. The laser controller (PDL-800-D, PicoQuant) and the APDs were connected to a counting card TCSPC (PicoHarp 300) for synchronization. Finally, the Sympho-Time 64 (PicoQuant) data acquisition software allowed the histograms to be recorded. The analysis of the traces was made considering exponential decays convoluted with the instrument response function (IRF) using a Levenberg-Marquardt numerical iteration algorithm [39]. The IRF was obtained with quenched sodium fluorescein in a pH = 10 phosphate buffer saturated with sodium iodide. The IRF showed a full width at half maximum of 200 ps. [60].

## 2.5. Fluorescence anisotropy measurements

The fluorescence anisotropy experiments were carried out with the same optical arrangement. The 485 nm excitation beam was sent through a film polarizer placed before dichroic separator. The emission was split into its parallel and perpendicular components with a polarizing beam splitter cube (Thorlabs) and sent to identical APDs. Finally, the fluorescence anisotropy evolution for each pigment was obtained from equation (1), where  $I_{\perp}(t)$  is the time dependent intensity of the perpendicular polarization component and  $I_{\parallel}(t)$  is the intensity in the parallel direction [61].

$$r(t) = \frac{I_{\parallel}(t) - I_{\perp}(t)}{I_{\parallel}(t) + 2I_{\perp}(t)} \quad (1)$$

## 2.6. Computational methods

The hydrodynamic contribution to the diffusional reorientation times of Pigment Red 149 and Pigment Red 179 were estimated using the respective molecular rotational diffusion coefficients. These calculations allowed for an approximation of the differences in rotational diffusion times of these two molecules which have similar emission lifetimes but different hydrodynamic volumes. These calculations give the dimensions of the three axial radii for the rotational relaxation coefficients (see below). We also calculated the transition moment directions and other geometric parameters for both molecules. The calculations were taken from structures obtained with the Gaussian 16 software package [62]. The ground state equilibrium geometries were optimized using the PBE0 functional and the 6–311++ G (d,p) basis set [63–66]. All calculations were performed with an implicit solvation model, PCM (Polarizable Continuum Model) in DMSO. The direction of the  $S_1-S_0$  transition dipoles were obtained with the TD-DFT method with the same functional and basis set [63–66]. For this, the equilibrium geometries were optimized in the first singlet excited state. The molecular volumes and axis sizes were calculated considering a constant electron density contour at 0.0035 electrons/bohr<sup>3</sup>. Details of the calculations of the hydrodynamic contribution to the overall rotational relaxation time can be found in the Supporting Info., page 10. [67,68].

### 3. Results and discussion

The four acrylic formulations chosen for this study are among the most common components for red coloring in murals and artistic works and are present in several examples from notable modern painters (see the Supporting Info. for a brief perspective in section Preface: Examples of red pigment used by modern artists) [8,18,45–48,69]. Applications of these acrylics are shown in Fig. 1. As can be seen, the dry paints span a range of red tonalities, but clearly show pairwise similarities between them. This highlights the importance of detecting the specific pigment used in each case. For example, the color in PR149 is similar to the one produced by the PV19 acrylic, while the PR179 one resembles the PR206 formulation.

As a starting point for the emission studies, the molecular identity of the analyzed pigments was confirmed by direct-analysis in real time mass spectrometry (DART). Additionally, for the commercial pigments PR206 and PV19, we recorded  $^1\text{H}$  NMR spectra in DMSO- $d_6$  solution as shown in the Supporting Info. This was done to determine the relative amounts of the components in the PR206 formulation (see below).

For all four acrylic paints, there is a single long-lived emissive species with distinct static emission signals at concentrations above  $10^{-5}$  M. All these samples also produce reproducible TCSPC traces at concentrations up to four orders of magnitude smaller. We start by describing the spectroscopic features of the emissive chromophores and show that in the acrylic samples the respective component is present as a unique long-lived emissive species.

#### 3.1. Steady-state spectroscopy

Fig. 2A to 2D show the static absorption, emission, and excitation spectra of the chromophores of this study. The insets include comparisons of the excitation and emission spectra of the pure chromophores with samples directly extracted from the respective acrylic films. The emission yields and other spectroscopic data are included in Table 1. The spectra of the perylene type chromophores, Pigment Red 149 (PR149) and Pigment Red 179 (PR179), are shown in Fig. 2A and B. These molecules are the only emissive species detected from the respective acrylic film extractions. As shown, the band position and progressions are nearly identical for the two molecules, differing only by a 4 nm shift. The emissions from dichloromethane solutions have maxima at 536 nm for the molecule with the dimethylphenylenic substitutions (PR149), and 532 nm in the dimethylperylimide compound (PR179). It should be mentioned that for the two perylenic systems, dichloromethane is the only solvent where significant concentrations can be achieved from extractions of the films.

Fig. 2C and D shows results for the PV19 and PR206 samples. For both these systems the only emissive component present in DMSO or dichloromethane extracts is the quinacridone pigment, whose spectrum is included in the main graph of Fig. 2C. The main graph of Fig. 2D contains the spectra from quinacridone isolated from the PR206 acrylic

formulation. From the characterization of the extract (see Figs. S10, S13 and S14 in the Supporting Info.), and also according to the manufacturer's formula, quinacridone is the only pigment in the PV19 case, while in the PR206 formulation, quinacridone is mixed with the quinonic form of the molecule (quinacridone-quinone) to adjust the color into a maroon tone [70]. For the PR206 acrylic samples, the quinonic molecule is highly insoluble and is not extracted from the films using dichloromethane, appearing only in the DMSO extractions as a minor component. This observation is consistent with a previous report with regards to the analysis of PR206 [71]. Furthermore, the quinacridone-quinone component does not show any appreciable fluorescence as shown in the inset of Fig. 2D which compares the purified quinacridone spectra with those of the PR206 extraction, showing a match between the excitation and emission signals of the extracts with quinacridone (this will be further supported even at concentrations at the  $10^{-9}$  M level through TCSPC measurements).

Figs. S11 to S14 in the Supporting Info. show the absorption spectra obtained directly from dissolving a small piece of the film of the acrylic formulation in the respective solvents. The absorption spectra of some of these acrylic formulations can differ from that of the pure compound due to the presence of additional components which are dispersed into the solutions. In particular, for the PR206 commercial formulation, the absorption spectrum in Fig. S14 actually shows the characteristic band of the quinacridone-quinone compound centered at 430 nm [71] overlapped with the absorption spectrum of the quinacridone molecule.

#### 3.2. Time-Correlated Single Photon measurements

The chromophores of this study have highly emissive first singlet excited states with decay times in the range of several nanoseconds. The TCSPC traces are typical of the respective chromophore and correspond to single exponential decays as we show in the following study which includes the concentration dependence of the traces. As we show, these concentrations can be several orders of magnitude smaller than those of the steady-state spectra.

Fig. 3A to 3D show the TCSPC traces from solutions of the pure pigments. The decays correspond to single exponentials of  $3.50 \pm 0.25$  ns for Pigment Red 149 (PR149) and  $3.90 \pm 0.29$  ns for Pigment Red 179 (PR179) in dichloromethane solutions. The quinacridone molecule also shows a single exponential decay with a much longer decay time of  $17.70 \pm 0.24$  ns in DMSO. In these measurements, the uncertainties were determined from the repetition of at least three independently prepared samples and TCSPC alignments and measurements.

We also characterized the emission decays for a series of dilutions from the samples extracted from films of the four acrylic formulations. The decays at several dilution levels are included in Fig. 4A to 4D. As a technical note, the confocal type of setup used for these determinations with the use of a 1.4 NA objective, allows for three to four orders of magnitude better sensitivity in comparison with arrangements which use a perpendicular excitation-detection setup with an imaging lens for

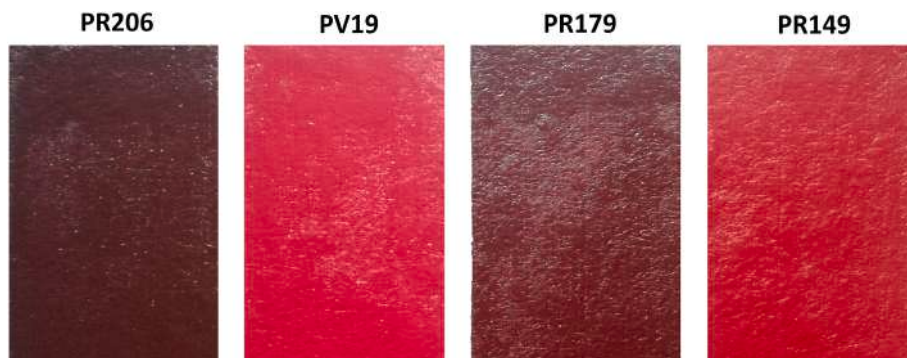
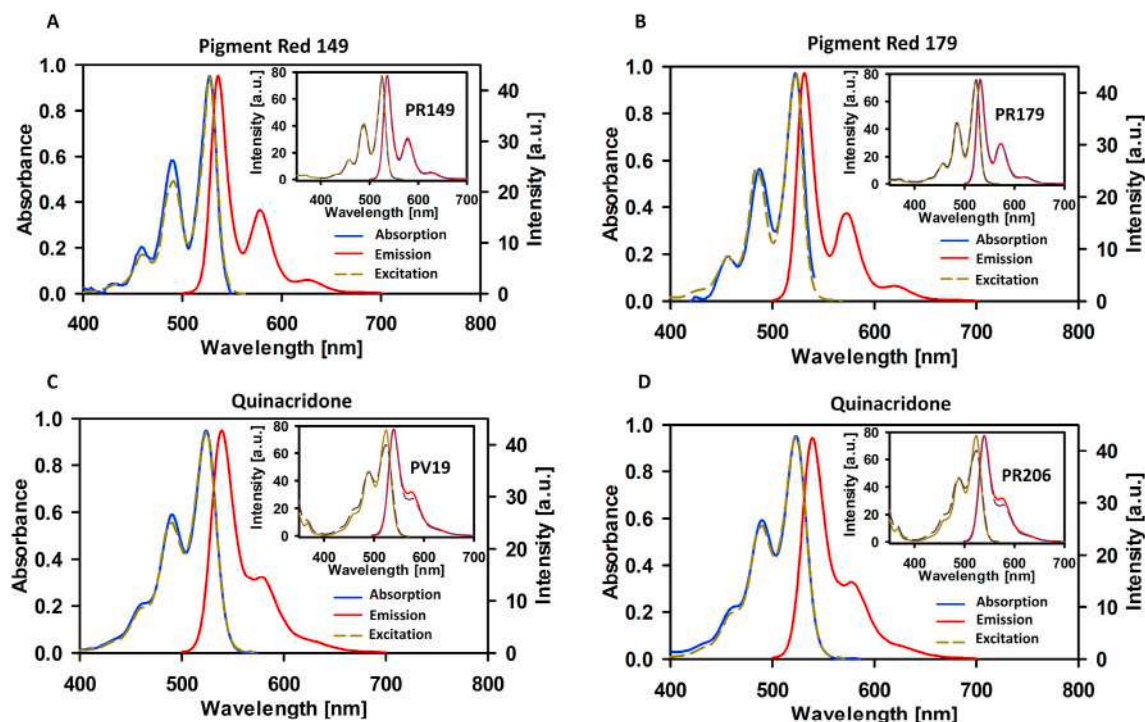


Fig. 1. Samples of acrylic paints used in this study. Acrylic formulations applied on a fiber cement panel are shown, each acrylic is indicated in the top label.



**Fig. 2.** Absorption (solid blue lines), emission (solid red lines) and excitation (dashed green lines) spectra of the pigments of this study. The insets show a comparison between the emission and excitation spectra of the pure pigments (solid lines) and the solutions that result from extractions from the films of the acrylic formulations (dark dashed lines). A) Pigment Red 149 and B) Pigment Red 179 in dichloromethane C) quinacridone and D) extracted quinacridone from the PR206 acrylic formulation in DMSO. The main graph in D) corresponds to the quinacridone molecule purified from the commercial formulation. The inset in D compares the emission and excitation spectra of the quinacridone molecule with that from the extracted sample from PR206. The excitation wavelength was 490 nm and the emission wavelength was 580 nm.

**Table 1**

Molar extinction coefficients  $\epsilon$  ( $\text{dm}^3\text{mol}^{-1}\text{cm}^{-1}$ ) at the maximum peak, and fluorescence yields  $\phi_f$  of the emissive pigments of this study.

	Absorption		Emission	
	$\lambda_{\text{max}}(\text{nm})$	$\epsilon(\text{dm}^3\text{mol}^{-1}\text{cm}^{-1})$	$\lambda_{\text{max}}(\text{nm})$	$\phi_f$
Pigment Red 149 (PR149)	527	11048 (490)	536	0.96
Pigment Red 179 (PR179)	523	2891 (490)	532	0.96
Quinacridone (PV19 and PR206)	524	7036 (490)	539	0.99

light collection (data not shown). We also determined that for this series of dilutions, fits to the convoluted exponential traces using the full time-trace of the data and careful measurement of the instrument response function for each experiment, produces more reliable identification of the exponential decay in comparison with fitting methods that focus only on the long-time part of the traces ( $t > 0.2$  times the decay constant). This is illustrated in Fig. S15 in the Supporting Info.

The concentration of the chromophores from the original extracts (0.4 mm by 0.4 mm of the acrylic film) using 2 mL of the respective solvent were determined from absorption measurements and are all in the range of  $10^{-5}$  to  $10^{-6}$  M. As can be seen, the solutions extracted from films of the acrylic formulations have an excellent correspondence with the decay times of the pure compounds and can easily be identified from the traces. The decay times from the convoluted single exponential fits correspond to the  $3.50 \pm 0.25$  ns decay of PR149 in dilutions down to the order of  $10^{-9}$  M, and down to the  $10^{-8}$  M level for the  $3.90 \pm 0.29$  ns decay of PR179. On the other hand, for PV19 samples, the  $17.70 \pm 0.24$  ns emission decay was reliably observed down to the order of  $10^{-9}$  M.

As mentioned, the PR206 formulation is composed of two chromophores, quinacridone and quinacridone-quinone [71–73]. As indicated in Fig. 2D, the emission and excitation spectra from PR206 extracts

shows that the quinacridone chromophore is the only emissive species upon 485 nm excitation. This is confirmed from the TCSPC measurements which clearly show that for extracts of films from PR206, the only decay time corresponds to the same  $17.70 \pm 0.24$  ns decay observed in quinacridone and in the PV19 samples. From this observation it can be concluded that the quinacridone-quinone molecule (see Fig. S14), with an absorption band at 430 nm does not possess a long-lived emissive  $S_1$  state. This is consistent with the presence of carbonyl groups in the quinone structure which promote efficient intersystem crossing into the triplet manifold of the molecule, therefore limiting the formation of the fluorescent state [74–76]. The single 17.70 ns decay indicates that even with the maroon color of the PR206 sample (which can be distinguished clearly from PV19 but easily confused with PR179), this commercial pigment can be readily identified. This decay is reliably detected down at least to  $10^{-9}$  M, although at such low concentrations the traces show a biexponential behavior where the long lifetime remains within experimental error of 17.70 ns (quinacridone). The additional lifetime corresponds to a fast sub-200 ps components which arises from scattering from the DMSO solution. Tables S2 to S5 in the Supporting Info. include the results of the observed decays for concentrations below the mentioned ones, where the traces start to deviate from those of the pure substances, indicating a limit for the identification of the characteristic time constant.

Next, we turn to the characterization of dried samples of the acrylic formulations deposited on the surface of different substrates. In large-format paintings such as murals, the possibility might arise to have microscopic samples of the dried material obtained from the edges of the mural or from small flakes [77,78]. Alternatively, a minimal amount of material can be obtained through the use of micro-swabs, either dry or infused with small amounts of a solvent. These kinds of samples can be used to produce solutions in a volume of the order of a few microliters [35–37,42,43].

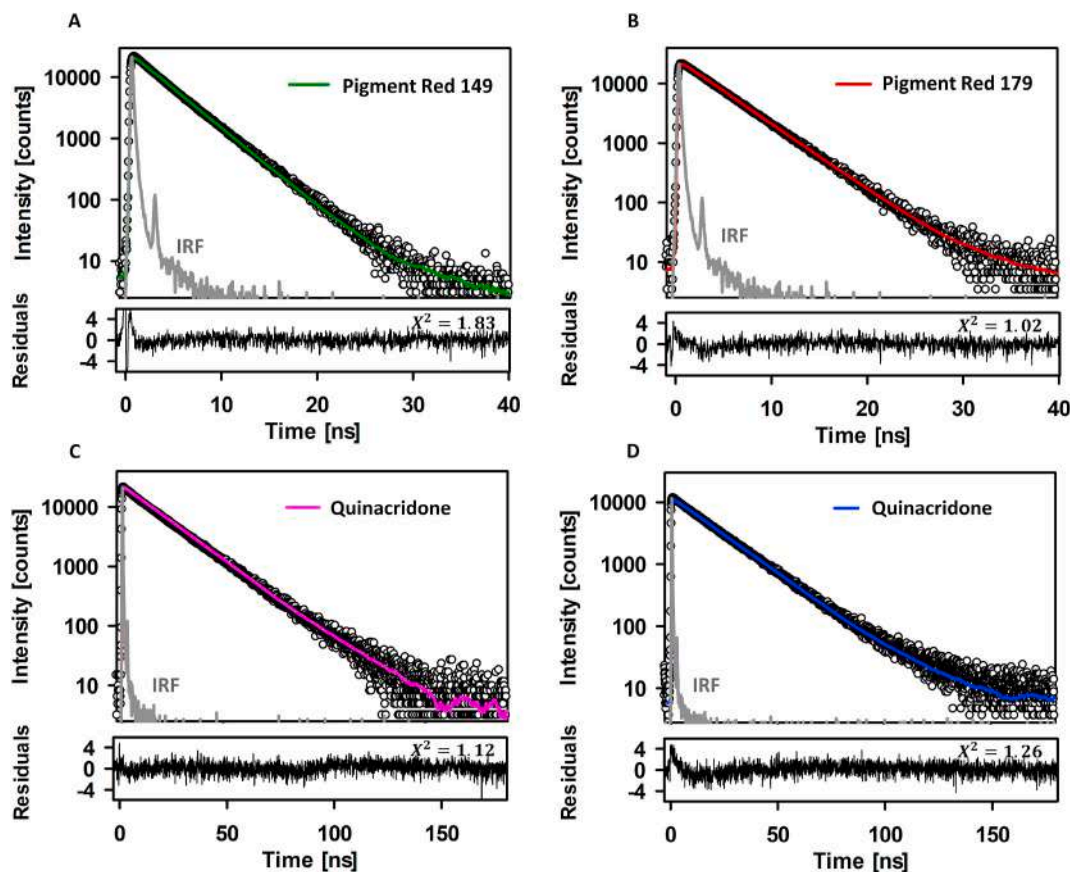


Fig. 3. TCSPC measurements of the pigments excited at 485 nm. A) Pigment Red 149 B) Pigment Red 179 C) quinacridone in PV19 and D) quinacridone in PR206. Convoluted fits are shown as colored lines, the instrumental response function (IRF) is shown in gray. Also, residuals and chi-squared values are shown at the bottom of TCSPC measurements.

We first carried out micro-swab sampling of the surface of the dry acrylic applications on fiber cement surfaces showing how it is indeed easy to identify the respective pigment from TCSPC measurements of a solution formed directly from this method. The procedure to obtain the samples is highlighted in Fig. 5 and in a video for which a link is included in the Supporting Info (see caption of Fig. S16). The respective decay traces of the four acrylics are included in Fig. S16. These traces show decay times well within the standard deviation of the pure pigment and the acrylic film extracts. The respective concentrations of these samples correspond approximately to  $10^{-7}$  M from the observed photon count rate. The decay results from the swabbing technique are summarized in Table S6.

Second, we attempted to determine which is the minimal solid fragment size (flake) which still can be used to detect the respective chromophore (see Fig. S2 in the Supporting Info. for images of the flakes). Once more, the sensitivity of TCSPC is highlighted in the measurements of the microscopic flakes. Figs. 6A to D shows the decay traces observed from different dry sample sizes using the FC substrate. For the other substrates, the plots are included in the Supporting Info. For sample sizes of 40  $\mu\text{m}$  lateral size (or likely smaller), the characteristic time constant of the excited state decay is distinguished unambiguously for the pigments and falls within the experimental uncertainty of the pure samples or the ones extracted from the films. These samples in all cases correspond to microscopic flakes which carry with them a certain amount of the substrate (plaster, etc.). The results of Fig. 6 support the idea that, for these dry micro-samples, the presence of substrate material does not impede the appropriate measurement of the lifetimes.

As a central issue for these measurements, it should be mentioned that, due to the small volumes, the use of dichloromethane as solvent does not give reproducible results for microscopic samples due to its

high volatility, which gradually changes the pigment concentration during the TCSPC measurements (1–5 min). This difficulty required a new scheme to disperse the pigment molecules for PR149 and PR179 which only can be initially dissolved in this solvent. A reliable scheme was to bring the initial extractions with dichloromethane into toluene. The toluene solution (after rapid evaporation of the dichloromethane component) produces reliable results for the TCSPC measurements since aggregation or precipitation does not take place to any extent in the time scale of the experiment. The toluene solutions show emission lifetimes that are different from those from dichloromethane, as expected, due to the change in the solvent environment ( $3.61 \pm 0.11$  ns for toluene vs  $3.50 \pm 0.25$  ns in dichloromethane for PR149; and  $4.10 \pm 0.18$  ns for toluene vs  $3.90 \pm 0.29$  ns in dichloromethane for PR179).

### 3.3. Fluorescence anisotropy decays

As an additional method to confirm the presence of specific pigments through their TCSPC traces, we measured the decay of the emission anisotropy  $r(t)$ , since the rotational diffusion in a specific solvent or mixture is also characteristic of the fluorophore. This can be taken as an advantage as we show next: Typically, for low viscosity solvents at room temperature the decay of the emission anisotropy occurs in the picoseconds time scale. Such times can fall within the instrumental response of most TCSPC setups which could make this an unreliable way to detect a pigment in the solution. However, upon adjustment of the solvent viscosity, the decay times for the emission anisotropies can easily be brought into the nanoseconds time range.

We have highlighted this strategy to differentiate chromophores by comparisons of the anisotropy decays of the two perylenic pigments of this study (Pigment Red 149 (PR149) and Pigment Red 179 (PR179)).

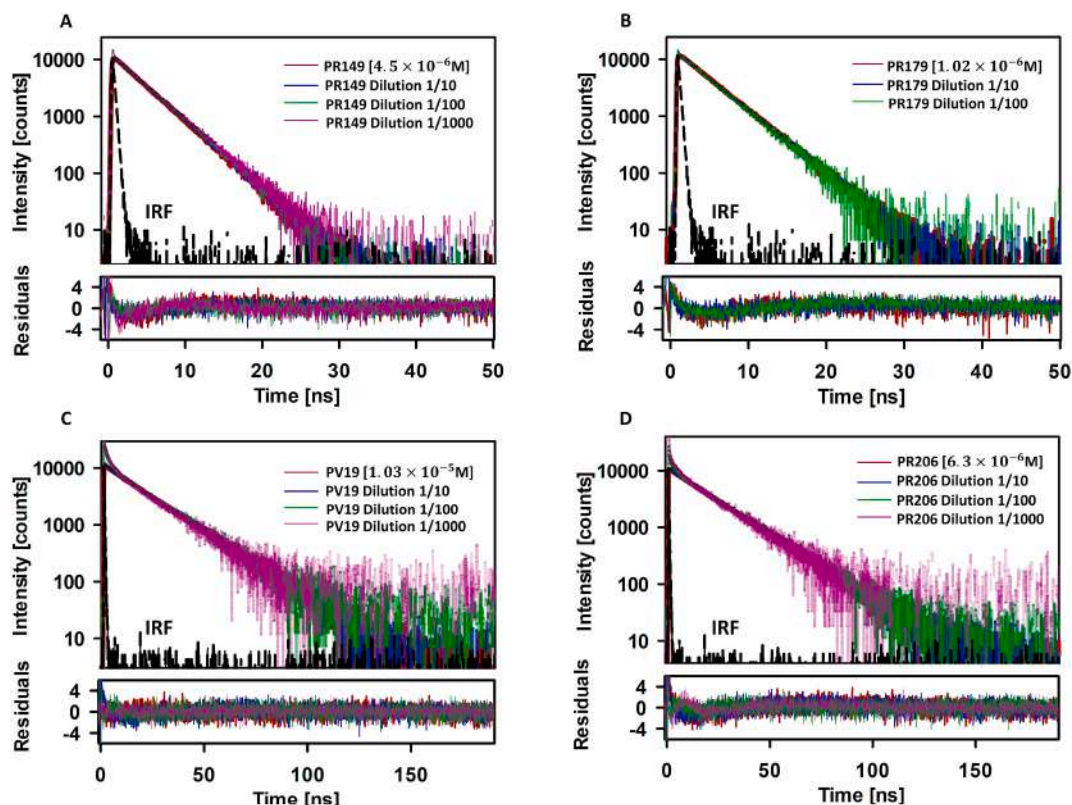


**Fig. 4.** TCSPC measurements at several dilution levels of extracts from films of the acrylic formulations. In all cases, the excitation wavelength was 485 nm. A) pigment PR149 and B) pigment PR179 in dichloromethane C) pigment PV19 and D) pigment PR206 in DMSO. The traces corresponding to the dilutions are shown as colored lines. The instrumental response function (IRF) is shown in black, and residuals are shown at the bottom of TCSPC measurements. The original concentration of each pigment was determined from the respective absorption coefficient.

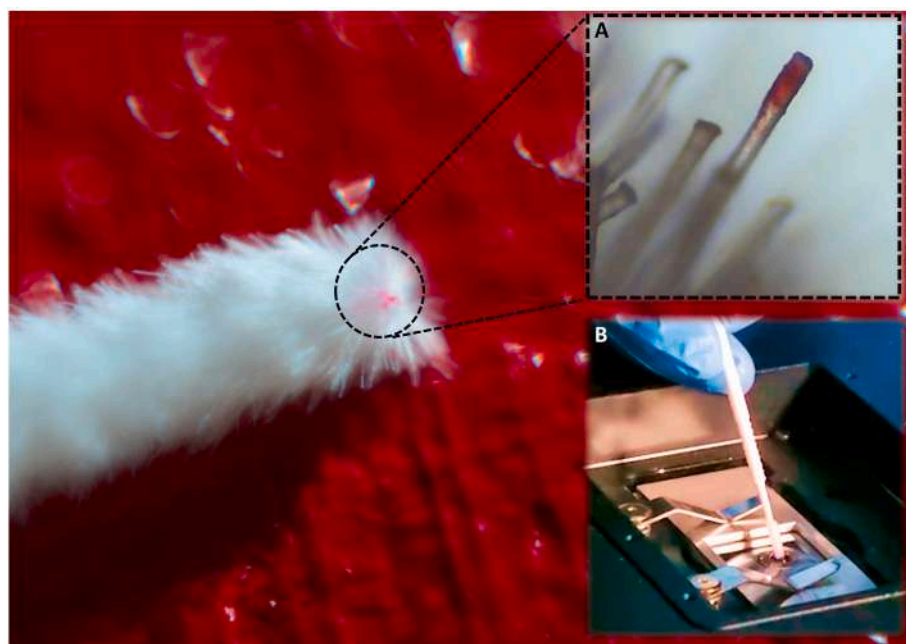


**Fig. 5.** Micro-swab sampling of dried surfaces of the acrylics deposited on fiber cement. The insets show A) micro-swab, image taken under a microscope with a 10× objective B) sample deposited in the surface of the observation slide where, previously, a 2 µL drop of the appropriate solvent was placed.

These two molecules have similar emission lifetimes making it difficult to differentiate them. The two molecules, however, differ significantly in their hydrodynamic properties despite having the same chromophoric core. On one hand, Pigment Red 149 has two dimethylphenyl groups at

the long axis ends of the molecule, while Pigment Red 179 only has methyl groups. Such structural differences suggest that the two systems will have different hydrodynamic contributions to their rotational diffusion coefficients. A series of solutions of increasing viscosity were

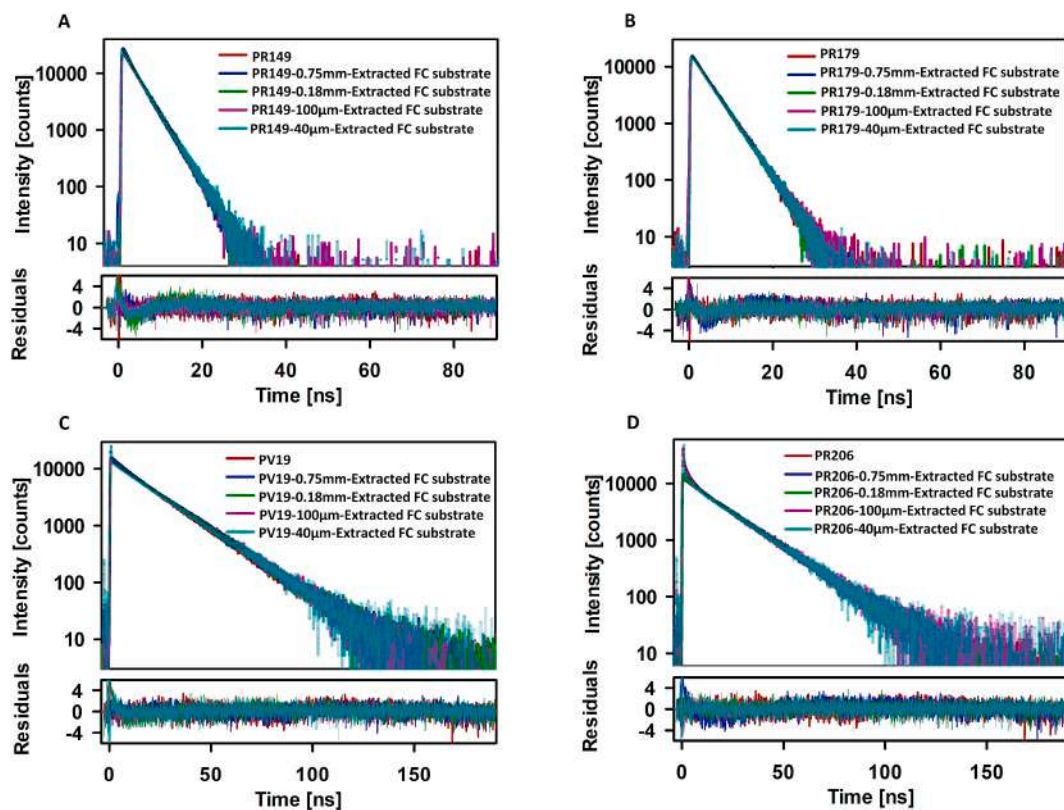


Fig. 6. TCSPC measurements for different sample sizes of dry acrylic paints applied on a fiber cement (FC) substrate. The solutions were excited with a wavelength of 485 nm. A) extracted pigment PR149 and B) extracted pigment PR179 in dichloromethane and then diluted in toluene C) extracted pigment PV19 and D) extracted pigment PR206 in DMSO. Residuals are shown at the bottom of the respective TCSPC measurements.

prepared as follows. Pigments were extracted with dichloromethane, then were transferred into DMSO as described previously for toluene. After complete evaporation of dichloromethane, from the stock DMSO solution, glycerin was added thus increasing its molar fraction in the mixture, from 0 to 0.79 in steps of 0.10 units. The experimental anisotropy traces are shown in Fig. 7. As can be seen, the  $r(t)$  decay traces and time constants evolve from a sub-nanosecond range (0.19 mol fraction of glycerin in DMSO) to more than 7 ns for the mixtures with the higher molar fraction of glycerin. The characteristic rotational relaxation times are included in Table 2 [61].

Importantly, not only the  $r(t)$  exponential decay times increase upon elevating the glycerin mole fractions, but also the difference between the  $r(t)$  decays of PR149 and PR179 varies gradually. This variation is also included in Table 2 as a percent difference in the  $r(t)$  decay times. As can be seen, for a glycerin mole fraction of 0.39, the difference is maximal:  $3.54 \pm 0.14$  ns for PR149 vs  $1.90 \pm 0.21$  ns for PR179. This example clearly indicates that anisotropy measurements (with a similar detection level as the TCSPC method) can be used to unambiguously differentiate between two molecules with the same chromophoric core (and therefore similar fluorescence decay times), but a different substitution pattern, which in turn result in differences in their rotational diffusion.

In order to further support the notion that the differences between the anisotropy decays in the PR149 vs PR179 samples are due to differences in their hydrodynamic friction, we have estimated their purely-hydrodynamic rotational relaxation times. The molecules' geometries were modelled as ellipsoids, and their diffusion coefficients were calculated from DFT studies considering electron density isosurfaces using standard procedures [71]. The direction of the transition dipole moment vectors of both molecules was obtained from TD-DFT calculations.

We made estimations of the hydrodynamic contributions to the rotational relaxation times following the method by Dutt et al. [68]; and

the solvent mixture viscosities were taken from the literature [67,79, 80]. Details of these calculations can be found in the Supporting Info., on page 10. As we show in the solid lines of the inset of Fig. 8, the two molecules differ significantly in their hydrodynamic contribution to friction. This is of course also reflected in the observed rotational relaxation times of the main graph of Fig. 8, although it is well known that solvents that contain glycerin have other sources of friction, including specific and electrostatic interactions, and therefore, the observed times are up to an order of magnitude smaller than the prediction of the simple hydrodynamic model (see Supporting Info. page 11) [61,81,82]. It should be noted that the Pigment Red 149 molecule has larger substituents at the end points of its long axis. This implies a larger hydrodynamic friction in comparison with the methyl groups in Pigment Red 179. In addition, Plotting the experimental rotational relaxation times as a function of the mixture viscosity according to:

$$\tau_{rot} = \frac{V_{eff}}{k_B T} \eta + \tau_{rot}^0 \quad (2)$$

gives a value of  $8.0 \times 10^3 \text{ \AA}^3$  for Pigment Red 149 and  $3.8 \times 10^3 \text{ \AA}^3$  for Pigment Red 179, highlighting the fact that these two molecules have different hydrodynamic volumes which result in clear differences in their observed rotational diffusion properties. Importantly, the differences in the molecular dimensions are due mainly to the long axis of the molecule which is parallel to the emission transition dipole moment. This feature in turn results on a large sensitivity of the rotational decays on the size of the long axis of the molecules [79]. Clearly, such structural variation induces significant differences in the experimental  $r(t)$  decay times which can be as large as 80% depending on the exact DMSO/glycerin mixture. In summary, the  $r(t)$  measurements clearly serve as an additional method to differentiate the two pigments which are otherwise very similar in their fluorescence lifetimes.

The anisotropy decay times of the PV19 and PR206 samples were

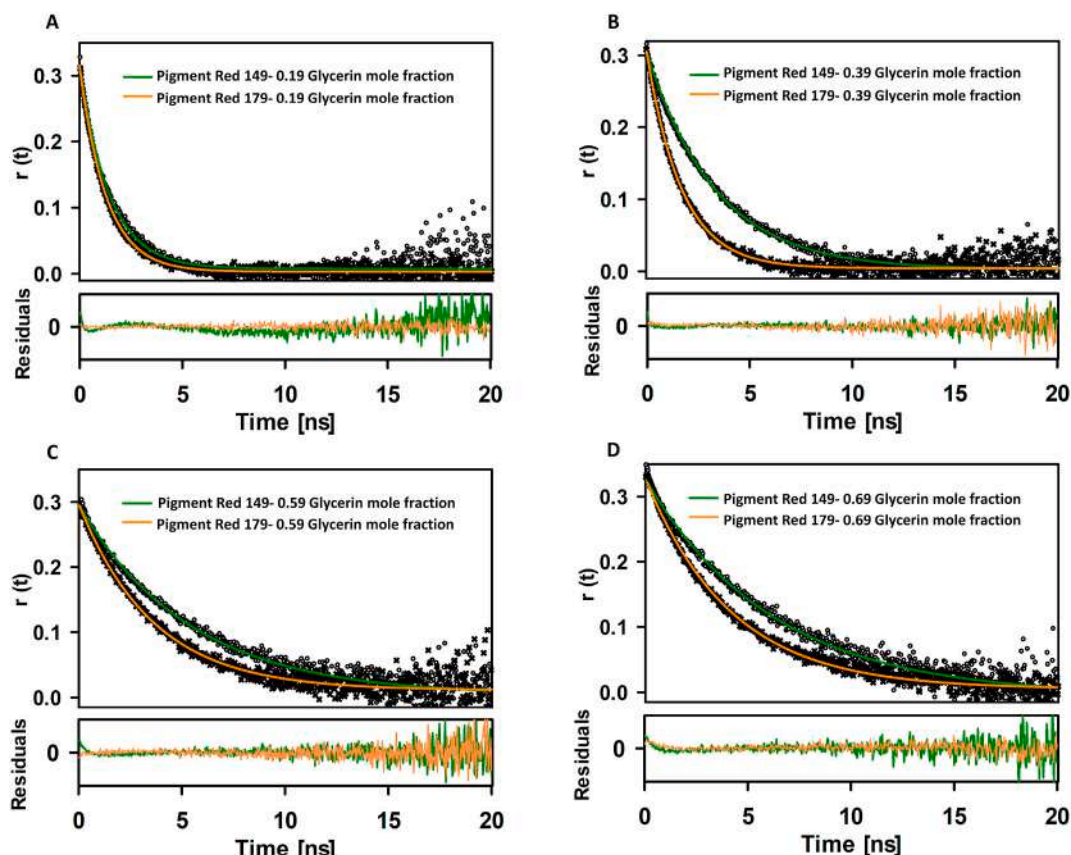


**Fig. 7.** Anisotropy ( $r(t)$ ) traces for extracts of PR149 and PR179 in glycerin-DMSO mixtures. A) 0.19 glycerin mole fraction B) 0.39 glycerin mole fraction. C) 0.59 glycerin mole fraction and D) 0.69 glycerin mole fraction. The excitation wavelength was 485 nm and residuals are shown at the bottom of the respective anisotropy ( $r(t)$ ) traces.

**Table 2**

Rotational relaxation times ( $\tau_{rot}$ ) of perylenes PR149 and PR179 in DMSO-glycerin mixtures obtained from single exponential fits to the fluorescence anisotropy decays. The percent difference column indicates the difference between the rotational relaxation times of the two molecules.

Glycerin mole fraction	PR149		PR179		Percent difference (%)
	$r(t=0)$	$\tau_{rot}(ns)$	$r(t=0)$	$\tau_{rot}(ns)$	
0.19	0.3	$1.57 \pm 0.11$	0.3	$1.40 \pm 0.14$	11.9
0.29	0.3	$2.15 \pm 0.23$	0.3	$1.44 \pm 0.12$	48.7
0.39	0.3	$3.54 \pm 0.14$	0.3	$1.90 \pm 0.21$	86.8
0.49	0.3	$4.14 \pm 0.19$	0.3	$2.63 \pm 0.17$	57.3
0.59	0.3	$5.66 \pm 0.27$	0.3	$3.63 \pm 0.23$	56.2
0.69	0.3	$7.58 \pm 0.21$	0.3	$4.52 \pm 0.25$	67.5
0.79	0.3	$9.00 \pm 0.18$	0.3	$5.68 \pm 0.20$	58.6

also determined. In these cases, the solvent mixture was formed directly with DMSO and glycerin. The respective time constants are included in Table 3. Fig. S20 shows the  $r(t)$  trace characteristic of pure quinacridone with a time of  $12.35 \pm 0.70$  ns. As shown in Table 3, the  $r(t)$  decay values are within uncertainty for the PV19 and PR206 samples. This is again consistent with the fact that quinacridone is the only emissive pigment in these formulations.

Finally, as a technical note for the anisotropy experiments, we

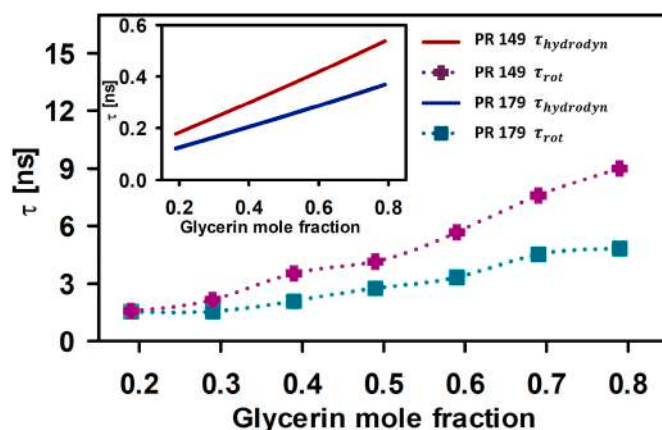


**Fig. 8.** Dotted lines with symbols: Experimentally determined rotational relaxation times ( $\tau_{rot}$ ) as a function of the glycerin mole fraction in DMSO-glycerin mixtures for Pigment Red 149 (PR149) and Pigment Red 179 (PR179). Inset: estimated hydrodynamic contribution to the rotational relaxation times ( $\tau_{hydrodyn}$ ) for the viscosity of the mixture. The respective calculations are included in the Supporting Info.

showed that the anisotropy decay times do not vary as a function of the objective's NA. Specifically, it is well known that different experimental  $r(t=0)$  values will be obtained for objectives with different NA's (with smaller  $r(t=0)$  values for the larger NA lenses) [83,84]. However, as we show in Figs. S21 and S22 for PV19 samples, the traces taken with three different lenses (with NA's ranging from 0.5 to 1.4), show the same  $r(t)$  decay times.

**Table 3**

Rotational relaxation times  $\tau_{rot}$  from single exponential fits to fluorescence anisotropy traces of quinacridone in PV19 and PR206.

Glycerin mole fraction	PV19		PR206	
	$r(t=0)$	$\tau_{rot}(ns)$	$r(t=0)$	$\tau_{rot}(ns)$
0.79	0.2	12.21 ± 0.75	0.2	12.59 ± 0.73

#### 4. Conclusions

We explored the emissive properties of red chromophores present in four representative acrylics. The objective of this study was to define a set of strategies to differentiate red pigments through the time resolution of their fluorescence signals. TCSPC is a high sensitivity technique which can be applied to the four acrylics. These red pigments can be identified from their decay times in concentrations as low as  $10^{-9}$  M. This method also allows for the detection of the pigments in microscopic samples of 40  $\mu$ m lateral size and those obtained through micro-swab sampling in representative substrates of murals. The use of confocal-type setups allows for the use of minimal volumes so that the chromophore concentration is relatively high.

These studies indicate that the problem of high volatility of the solvents that facilitate the pigment extraction but hinder the TCSPC measurements can be solved by transferring the sample into a different solvent system where the solution is stable in the time scale of the experiments. Also, using the same set up but allowing for parallel and perpendicular polarization detections, together with highly viscous solvent mixtures, the chromophores can be identified from their anisotropy decay times. The anisotropy measurements are highly dependent on the molecular structure and therefore can differentiate molecules that have similar fluorescence decays but different hydrodynamic behavior for reorientation. With this strategy, the time constants of the anisotropy decays can be brought to have differences of more than 50% for chromophores which have fluorescence lifetimes times within 5% of each other. The procedures highlighted in this study are the initial steps to implement identification procedures for emissive chromophores commonly used in modern paintings. The main objective of this contribution was to study the effects of sample concentration, sample nature and dimensions, and acquisition method, to serve as the basis of a comprehensive study with a much broader set of pigments and mixtures. These strategies also can promote the integration of research groups with experience in time-resolved emission measurements with experts in cultural heritage and maintenance of murals and paintings for conservation efforts.

#### Notes

The authors declare no competing financial interest.

#### Author statement

Cadena-Caicedo Andrea, Conceptualization, Methodology, Data Curation, Writing, Reviewing and Editing. González-Gutiérrez Mario, Methodology, implementation of Time-resolved Fluorescence. Guzmán-Méndez Óscar, Methodology, purification and identification of organic compounds. M. Reza Mariana, Methodology, implementation of anisotropy measurements. Durán-Hernández Jesús. Prediction of hydrodynamic properties of two compounds. Jorge Peon, Conceptualization, Writing- Reviewing and Editing, Funding.

#### Declaration of competing interest

The authors declare that they have no known competing financial interests or personal relationships that could have appeared to influence the work reported in this paper.

#### Acknowledgment

Authors acknowledge CONACyT-Mexico grant Fronteras de la Ciencia 2019–51496, CONACyT-Mexico 285722, and PAPIIT/DGAPA/UNAM IG200621 for financial support, DGTIC-UNAM project LANCAD-UNAM-DGTIC-210 for computer time. The authors are thankful for the NMR measurements at LURMN and DART spectra at LEM Mass Spectrometry Laboratory, and Laboratorio Nacional de Ciencias para la Investigación y Conservación del Patrimonio Cultural at UNAM's Instituto de Química.

#### Appendix A. Supplementary data

Supplementary data to this article can be found online at <https://doi.org/10.1016/j.jlumin.2022.118913>.

#### References

- [1] L. Rainer, L. Manning, The Siqueiros Legacy, Challenges of Conserving the Artist's Monumental Murals: Proceedings of a Symposium Organized by the Getty Conservation Institute, Getty Conservation Institute, 2013.
- [2] M. Rooney, T. Meldrum, Effect of pigment concentration on NMR relaxometry in acrylic paints, *Magn. Reson. Chem.* 58 (2020) 880–888.
- [3] M. Aceto, Pigments — the palette of organic colourants in wall paintings, *Archaeol. Anthropol. Sci.* 3 (2021) 1–23.
- [4] J. Gutiérrez, N. Roukes, *Painting with Acrylics*, vol. 9, Watson-Guipill Publications, 1966.
- [5] R.J.H. Clark, Pigment identification by spectroscopic means: an arts/science interface, *Compt. Rendus Chem.* 5 (2002) 7–20.
- [6] A. Romani, C. Clementi, C. Miliani, G. Favaro, Fluorescence spectroscopy: a powerful technique for the noninvasive characterization of artwork, *Acc. Chem. Res.* 43 (2010) 837–846.
- [7] A.V. Whitney, F. Casadio, R.P. Van Duyne, Identification and characterization of artists' red dyes and their mixtures by surface-enhanced Raman spectroscopy, *Appl. Spectrosc.* 61 (2007) 994–1000.
- [8] A.D. Squires, M. Kelly, R.A. Lewis, Terahertz analysis of quinacridone pigments, *J. Infrared, Millim. Terahertz Waves* 38 (2017) 314–324.
- [9] A. Nevin, et al., Time-resolved photoluminescence spectroscopy and imaging: new approaches to the analysis of cultural heritage and its degradation, *Sensors* 14 (2014) 6338–6355.
- [10] M. Ghirardello, et al., Photoluminescence imaging of modern paintings: there is plenty of information at the microsecond timescale, *Microchem. J.* 154 (2020) 104618.
- [11] A. Dal Fovo, et al., Fluorescence lifetime phasor analysis and Raman spectroscopy of pigmented organic binders and coatings used in artworks, *Appl. Sci.* 12 (2022).
- [12] M. Longoni, A. Freschi, N. Cicala, S. Bruni, Non-invasive identification of synthetic organic pigments in contemporary art paints by visible-excited spectrofluorimetry and visible reflectance spectroscopy, *Spectrochim. Acta Part A Mol. Biomol. Spectrosc.* 229 (2020).
- [13] J. Wouters, High performance liquid chromatography of anthraquinones: analysis of plant and insect extracts and dyed textiles, *Stud. Conserv.* 30 (1985) 119–128.
- [14] J. Sanyova, Mild extraction of dyes by hydrofluoric acid in routine analysis of historical paint micro-samples, *Microchim. Acta* 162 (2008) 361–370.
- [15] X. Zhang, R.A. Laursen, Development of mild extraction methods for the analysis of natural dyes in textiles of historical interest using LC-diode array detector-MS, *Anal. Chem.* 77 (2005) 2022–2025.
- [16] M.P. Colombini, A. Andreotti, G. Lanterna, M. Rizzi, A novel approach for high selective micro-sampling of organic painting materials by Er:YAG laser ablation, *J. Cult. Herit.* 4 (2003) 355–361.
- [17] P. Gottschaller, et al., *The Evolution of Lucio Fontana's Painting Materials*, vol. 57, 2012, pp. 76–91.
- [18] S.Q. Lomax, Phthalocyanine and quinacridone pigments: their history, properties and use, *Stud. Conserv.* 50 (2005) 19–29.
- [19] I.M. Cortea, et al., Characterization of Spray Paints Used in Street Art Graffiti by a Non-destructive Multi-Analytical Approach Employed in the Work of Representative Artists Such as, 2020, pp. 1–12.
- [20] L. Pronti, A.C. Felici, M. Me, C. Vieillescazes, M. Piacentini, Spectral Behavior of White Pigment Mixtures Using Reflectance, Ultraviolet — Fluorescence Spectroscopy, and Multispectral Imaging, 2017, pp. 1–10, 0.
- [21] B. Guineau, Non-destructive analysis of organic pigments and dyes using Raman microprobe, microfluorometer or absorption microspectrophotometer, *Stud. Conserv.* 34 (1989) 38–44.
- [22] F.W. Billmeyer, R. Kumar, M. Saltzman, Identification of Organic Colorants in Art Objects by Solution Spectrophotometry: Pigments vol. 58, 1981, pp. 307–313.
- [23] E.S.B. Ferreira, A.N. Hulme, H. McNab, A. Quye, The natural constituents of historical textile dyes, *Chem. Soc. Rev.* 33 (2004) 329–336.
- [24] Z. Bosakova, K. Stulik, P. Novotna, K. Stulik, High-performance liquid chromatographic determination of some anthraquinone and naphthoquinone dyes occurring in historical textiles, *J. Chromatogr. A* 863 (1999) 235–241.
- [25] J.C. Shearer, D.C. Peters, The art of FTIR microsampling, *Fourier Comput. Infrared Spectrosc.* (1985) 285, 0553.

- [26] S.M. Halpine, An improved dye and lake pigment analysis method for high-performance liquid chromatography and diode-array detector, *Stud. Conserv.* 41 (1996) 76–94.
- [27] L. Razaely, S. Héron, W. Nowik, A. Tchaplá, Optimisation of ESI-MS detection for the HPLC of anthraquinone dyes, *Dyes Pigments* 77 (2008) 191–203.
- [28] J. Zucker, National gallery technical bulletin, *Color Res. Appl.* 26 (2005).
- [29] A. Romani, et al., Portable equipment for luminescence lifetime measurements on surfaces, *Appl. Spectrosc.* 62 (2008) 1395–1399.
- [30] I. Degano, E. Ribechini, F. Modugno, M.P. Colombini, Analytical methods for the characterization of organic dyes in artworks and in historical textiles, *Appl. Spectrosc. Rev.* 44 (2009) 363–410.
- [31] D. Anglos, et al., Laser-induced fluorescence in artwork diagnostics: an application in pigment analysis, *Appl. Spectrosc.* 50 (1996) 1331–1334.
- [32] G. Poldi, S. Caglio, Phthalocyanine identification in paintings by reflectance spectroscopy, *Lab. In Situ Stud.* 114 (2013) 929–935, 1.
- [33] C. Clementi, et al., Vibrational and electronic properties of painting lakes, *Appl. Phys. Mater. Sci. Process* 92 (2008) 25–33.
- [34] G. Verri, C. Clementi, D. Comelli, S. Cather, F. Piqué, Correction of ultraviolet-induced fluorescence spectra for the examination of polychromy, *Appl. Spectrosc.* 62 (2008) 1295–1302.
- [35] K. Kahrim, et al., The application of in situ mid-FTIR fibre-optic reflectance spectroscopy and GC-MS analysis to monitor and evaluate painting cleaning, *Spectrochim. Acta Part A Mol. Biomol. Spectrosc.* 74 (2009) 1182–1188.
- [36] A. Sarmiento, et al., Classification and identification of organic binding media in artworks by means of Fourier transform infrared spectroscopy and principal component analysis, *Anal. Bioanal. Chem.* 399 (2011) 3601–3611.
- [37] G. Piñar, K. Sterflinger, Natural sciences at the service of art and cultural heritage: an interdisciplinary area in development and important challenges, *Microb. Biotechnol.* 14 (2021) 806–809.
- [38] B. Bao, et al., Recent Advances in Microfluidics-Based Chromatography — A Mini Review, vols. 1–19, 2021.
- [39] D. O'Connor, D. Phillips, *Time-correlated Single Photon Counting*, Academic Press, 2012.
- [40] L.M. Hirvonen, K. Suhling, Fast timing techniques in FLIM applications, *Front. Physiol.* 8 (2020) 1–20.
- [41] W. Becker, *Advanced Time-Correlated Single Photon Counting Techniques*, Springer Berlin Heidelberg, 2005.
- [42] S. Kamanna, J. Henry, N. Voelcker, A. Linacre, K. Paul Kirkbride, A complementary forensic 'proteo-genomic' approach for the direct identification of biological fluid traces under fingernails, *Anal. Bioanal. Chem.* 410 (2018) 6165–6175.
- [43] A. Moussa, M. Badawy, N. Saber, Chromatic alteration of Egyptian blue and Egyptian green pigments in pharaonic late period tempera murals, *Sci. Cult.* 7 (2021) 1–15.
- [44] P.K. Zarzycki, M.M. Ślaogonekczka, M.B. Zarzycka, E. Włodarczyk, M.J. Baran, Application of micro-thin-layer chromatography as a simple fractionation tool for fast screening of raw extracts derived from complex biological, pharmaceutical and environmental samples, *Anal. Chim. Acta* 688 (2011) 168–174.
- [45] C.A. Menke, R. Rivenc, T. Learner, The use of direct temperature-resolved mass spectrometry (DTMS) in the detection of organic pigments found in acrylic paints used by Sam Francis, *Int. J. Mass Spectrom.* 284 (2009) 2–11.
- [46] C. Defeyt, J. Mazurek, A. Zebala, D. Burchett-Lere, Insight into Sam Francis' painting techniques through the analytical study of twenty-eight artworks made between 1946 and 1992, *Appl. Phys. Mater. Sci. Process* 122 (2016) 1–6.
- [47] Y. Jin, *An Examination of the Place of Fresco in Contemporary Art Practice*, PhD thesis, Univ. Arts, London, 2004.
- [48] N.C. Scherrer, Z. Stefan, D. Francoise, F. Annette, K. Renate, Synthetic organic pigments of the 20th and 21st century relevant to artist's paints: Raman spectra reference collection, *Spectrochim. Acta Part A Mol. Biomol. Spectrosc.* 73 (2009) 505–524.
- [49] J. Mizuguchi, K. Tojo, Electronic structure of perylene pigments as viewed from the crystal structure and excitonic interactions, *J. Phys. Chem. B* 106 (2002) 767–772.
- [50] T. Sakamoto, C. Pac, A 'green' route to perylene dyes: direct coupling reactions of 1,8-naphthalimide and related compounds under mild conditions using a 'new' base complex reagent, t-BuOK/DBN, *J. Org. Chem.* 66 (2001) 94–98.
- [51] E. Del Puerto, C. Domingo, J.V. García Ramos, S. Sanchez-Cortes, Adsorption study and detection of the high performance organic pigments quinacridone and 2,9-dimethylquinacridone on Ag nanoparticles by surface-enhanced optical spectroscopy, *Langmuir* 30 (2014) 753–761.
- [52] T. Tsutsui, S. Kusaba, M. Yamashina, M. Akita, M. Yoshizawa, Open versus closed polyaromatic nanocavity: enhanced host abilities toward large dyes and pigments, *Chem. Eur. J.* 25 (2019) 4320–4324.
- [53] ASTM, Standard practices for producing films of uniform thickness of paint, *Coating Relat. Prod. Test Panels* 1. i (2018) 9.
- [54] A.T. Rhys Williams, S.A. Winfield, J.N. Miller, Relative fluorescence quantum yields using a Computer-controlled luminescence spectrometer, *Analyst* 108 (1983) 1067–1071.
- [55] J.V. Morris, M.A. Mahaney, J.R. Huber, Fluorescence quantum yield determinations. 9,10-Diphenylanthracene as a reference standard in different solvents, *J. Phys. Chem.* 80 (1976) 969–974.
- [56] M. Taniguchi, H. Du, J.S. Lindsey, PhotochemCAD 3: diverse modules for photophysical calculations with multiple spectral databases, *Photochem. Photobiol.* 94 (2018) 277–289.
- [57] J. Rodríguez-Romero, et al., Fluorophore release from a polymethinic photoremovable protecting group through a nonlinear optical process, *ChemPhotoChem* 1 (2017) 397–407.
- [58] L. Gutiérrez-Arzaluz, R. López-Arteaga, F. Cortés-Guzmán, J. Peon, Nitrate fluorophore formation upon two-photon excitation of an azide with extended conjugation, *J. Phys. Chem. B* 121 (2017) 9910–9919.
- [59] R. López-Arteaga, J. Peon, Ultrafast photoluminescence kinetics from hot excitonic states in CdSe nanocrystals, *J. Phys. Chem. C* 122 (2018) 26698–26706.
- [60] M. Liu, et al., Instrument response standard in time-resolved fluorescence spectroscopy at visible wavelength: quenched fluorescein sodium, *Appl. Spectrosc.* 68 (2014) 577–583.
- [61] J.R. Lakowicz, *Principles of Fluorescence Spectroscopy*, third ed., Springer, New York, USA, 2006. Springer: New York.
- [62] M.J. Frisch, et al., G16\_a03. Gaussian 16, Revision A.03, Gaussian, Inc., Wallin, 2016.
- [63] C.A. Guido, S. Knecht, J. Kongsted, B. Mennucci, Benchmarking time-dependent density functional theory for excited state geometries of organic molecules in gas-phase and in solution, *J. Chem. Theor. Comput.* 9 (2013) 2209–2220.
- [64] D. Jacquemin, V. Wathelet, E.A. Perpète, C. Adamo, Extensive TD-DFT benchmark: singlet-excited states of organic molecules, *J. Chem. Theor. Comput.* 5 (2009) 2420–2435.
- [65] M. Oltean, et al., Absorption spectra of PTCDI: a combined UV-Vis and TD-DFT study, *Spectrochim. Acta Part A Mol. Biomol. Spectrosc.* 97 (2012) 703–710.
- [66] M. Fortino, et al., On the simulation of vibrationally resolved electronic spectra of medium-size molecules: the case of styryl substituted BODIPYs, *Phys. Chem. Chem. Phys.* 21 (2019) 3512–3526.
- [67] M. Esquivelzeta-Rabell, J. Peon, G. Cuevas, Rotational diffusion of dihydroxy coumarins: effect of OH groups and their relative position on solute-solvent interactions, *J. Phys. Chem. B* 113 (2009) 8599–8606.
- [68] G.B. Dutt, T.K. Ghanty, Is molecular rotation really influenced by subtle changes in molecular shape? *J. Chem. Phys.* 121 (2004) 3625–3631.
- [69] M.B. Kasiri, N.A. Babaylou, H. Zandkarimi, Photo-oxidative stability of a series of red acrylic paints, *Prog. Color. Color. Coating* 7 (2014) 177–185.
- [70] Kremer Pigmente GmbH & Co, KG, Quinacridone Chestnut Brown, PR 206, 2016. SDS No. 23480. accessed June 29, 2021 Aichstetten, Germany.
- [71] E. Del Puerto, S. Sánchez-Cortés, J.V. García-Ramos, C. Domingo, Solution SERS of an insoluble synthetic organic pigment-quinacridone quinone-employing calixarenes as dispersive cavitands, *Chem. Commun.* 47 (2011) 1854–1856.
- [72] C. Binant, A. Lautie, Identification of quinacridone pigment mixtures using resonance Raman microspectrometry, *Appl. Spectrosc.* 43 (1989) 851–855.
- [73] S.Q. Lomax, The application of x-ray powder diffraction for the analysis of synthetic organic pigments. Part 1: dry pigments, *J. Coating Technol. Res.* 7 (2010) 331–346.
- [74] E.F. Plaza-Medina, W. Rodríguez-Córdoba, Peon, J. Role of upper triplet states on the photophysics of nitrated polyaromatic compounds: 51 lifetimes of singly nitrated pyrenes, *J. Phys. Chem.* 115 (2011) 9782–9789.
- [75] M.A. El-Sayed, Spin-orbit coupling and the radiationless processes in nitrogen heterocycles, *J. Chem. Phys.* 38 (1963) 2834–2838.
- [76] S.K. Lower, M.A. El-Sayed, The triplet state and molecular electronic processes in organic molecules, *Chem. Rev.* 66 (1966) 199–241.
- [77] R. White, The application of gas-chromatography to the identification of waxes, *Stud. Conserv.* 23 (1978) 57–68.
- [78] A. Mejía-González, et al., NMR and other molecular and elemental spectroscopies for the characterization of samples from an outdoor Mural painting by Siqueiros, *Spectrochim. Acta Part A Mol. Biomol. Spectrosc.* 274 (2022) 121073.
- [79] G.B. Dutt, S. Doraiswamy, Picosecond reorientational dynamics of polar dye probes in binary aqueous mixtures, *J. Chem. Phys.* 96 (1992) 2475–2491.
- [80] R.S. Hartman, W.M. Konitsky, D.H. Waldeck, Y.J. Chang, E.W. Castner, Probing solute – solvent electrostatic interactions: rotational diffusion studies of 9,10-disubstituted anthracenes, *J. Chem. Phys.* 106 (1997) 7920–7930.
- [81] C.R. Mateo, et al., Rotational dynamics of 1,6-diphenyl-1,3,5-hexatriene and derivatives from fluorescence depolarization, *J. Phys. Chem.* 97 (1993) 3486–3491.
- [82] E.F. Gudgin Templeton, E.L. Quitevis, G.A. Kenney-Wallace, Picosecond reorientational dynamics of resorufin: correlations of dynamics and liquid structure, *J. Phys. Chem.* 89 (1985) 3238–3243.
- [83] F. Ströhl, H.H.W. Wong, C.E. Holt, C.F. Kaminski, Total internal reflection fluorescence anisotropy imaging microscopy: setup, calibration, and data processing for protein polymerization measurements in living cells, *Methods Appl. Fluoresc.* 6 (2018).
- [84] D. Axelrod, Carbocyanine dye orientation in red cell membrane studied, *Biophys. J.* 26 (1979) 557–573.